Magnetic Resonance in Medicine 66:1674–1681 (2011)

Compressed-Sensing Motion Compensation (CosMo): A Joint Prospective–Retrospective Respiratory Navigator for Coronary MRI

Mehdi H. Moghari,[1] Mehmet Akçakaya,[1] Alan O'Connor,[1,2] Tamer A. Basha,[1] Michele Casanova,[1] Douglas Stanton,[3] Lois Goepfert,[1] Kraig V. Kissinger,[1] Beth Goddu,[1] Michael L. Chuang,[1] Vahid Tarokh,[2] Warren J. Manning,[1,4] and Reza Nezafat[1]*

Prospective right hemidiaphragm navigator (NAV) is commonly used in free-breathing coronary MRI. The NAV results in an increase in acquisition time to allow for resampling of the motion-corrupted *k*-space data. In this study, we are presenting a joint prospective–retrospective NAV motion compensation algorithm called compressed-sensing motion compensation (CosMo). The inner *k*-space region is acquired using a prospective NAV; for the outer *k*-space, a NAV is only used to reject the motion-corrupted data without reacquiring them. Subsequently, those unfilled *k*-space lines are retrospectively estimated using compressed sensing reconstruction. We imaged right coronary artery in nine healthy adult subjects. An undersampling probability map and sidelobe-to-peak ratio were calculated to study the pattern of undersampling, generated by NAV. Right coronary artery images were then retrospectively reconstructed using compressed-sensing motion compensation for gating windows between 3 and 10 mm and compared with the ones fully acquired within the gating windows. Qualitative imaging score and quantitative vessel sharpness were calculated for each reconstruction. The probability map and sidelobe-to-peak ratio show that the NAV generates a random undersampling *k*-space pattern. There were no statistically significant differences between the vessel sharpness and subjective score of the two reconstructions. Compressed-sensing motion compensation could be an alternative motion compensation technique for free-breathing coronary MRI that can be used to reduce scan time. Magn Reson Med 66:1674–1681, 2011. © 2011 Wiley Periodicals, Inc.

Key words: coronary MRI; motion correction; diaphragmatic navigators; compressed sensing

[1]Department of Medicine (Cardiovascular Division), Beth Israel Deaconess Medical Center, Harvard Medical School, Boston, Massachusetts, USA.

[2]School of Engineering and Applied Sciences, Harvard University, Cambridge, Massachusetts, USA.

[3]Philips Research North America, Briarcliff Manor, New York, USA.

[4]Department of Radiology, Harvard Medical School and Beth Israel Deaconess Medical Center, Boston, Massachusetts, USA.

Grant sponsor: NIH; Grant numbers: R01EB008743-01A2, UL1 RR025758-01; Grant sponsor: AHA; Grant number: SDG-0730339N; Grant sponsor: Harvard Clinical and Translational Science Center, from the National Center for Research Resources; Grant sponsor: Natural Sciences and Engineering Research Council of Canada (NSERC; fellowship support)

*Correspondence to: Reza Nezafat, PhD, Beth Israel Deaconess Medical Center, 330 Brookline Avenue, Boston, Massachusetts 02215.
E-mail: rnezafat@bidmc.harvard.edu

Received 30 October 2010; revised 22 January 2011; accepted 11 March 2011.

DOI 10.1002/mrm.22950
Published online 10 June 2011 in Wiley Online Library (wileyonlinelibrary.com).

Respiratory and cardiac motions are the main challenges of high-resolution coronary MRI (1). For cardiac motion, a patient's specific rest period during the cardiac cycle is commonly used (2). While breath-hold acquisitions have been previously used in coronary MRI (3,4), the limited breath-hold duration constraints spatial resolution and the clinical applicability of this approach. Despite several advances over the past two decades, respiratory motion still remains a major challenge.

Various methods exist for respiratory motion monitoring and compensation. Respiratory navigators (NAVs) were developed a decade ago and have been continuously refined to become the most reliable respiratory motion compensation technique for free-breathing coronary MRI (5–7). A two-dimensional (2D) pencil beam or spin echo with orthogonal planes for excitation and refocusing, positioned on the right hemidiaphragm, is used to monitor the respiratory motion. In prospective acceptance–rejection NAV gating (8,9), the *k*-space segment, acquired immediately following the NAV, is accepted if the NAV is within a prespecified acceptance gating window. Otherwise, data are discarded and reacquired in the next cardiac cycle. This results in an acceptance efficiency of 30–80%. A larger gating window improves data acquisition efficiency, albeit with the penalty of accepting more motion-corrupted *k*-space. Multiple methods have been proposed to improve NAV motion detection capability and acquisition efficiency which are comprehensively reviewed by Scott et al. (1). Examples of such advancements include fat NAV as a surrogate for direct coronary motion (10,11), leading and trailing NAV (7), and continuously adaptive windowing strategy to improve acquisition efficiency (12).

Image- or projection-based methods have also been presented to compensate for respiratory motion (13–15). In projection-based techniques, the motion of the heart directly measured from acquired raw data is used to calculate the respiratory motion. In image-based techniques, a low-resolution image is commonly extracted from the central portion of *k*-space and used for retrospectively compensating the respiratory motion (16–18). Rigid body and affine transformations can also be used for prospectively correcting the respiratory motion and increasing the gating window and efficiency rate (19–21). While prospective acquisition is commonly used for coronary MRI, there have been also some studies of using a retrospective NAV gating with the aim of improving gating efficiency or completion of scan in a fixed amount of time (22,23).

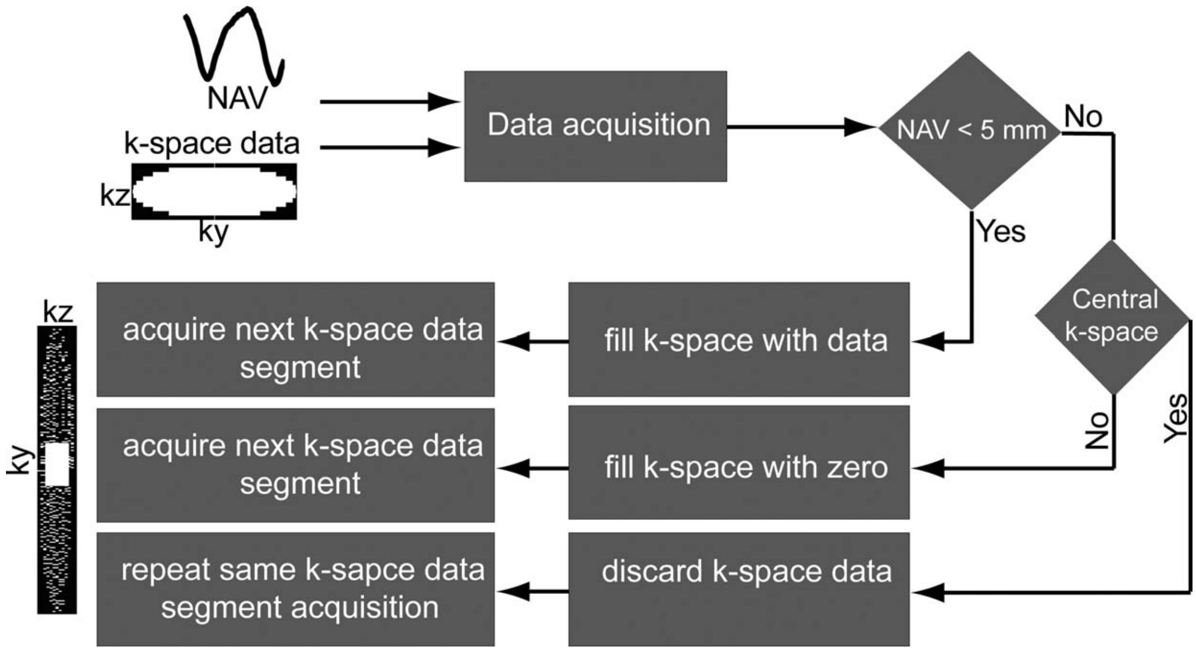

FIG. 1. Schematic of the proposed joint retrospective–prospective NAV scheme for CosMo: inner *k*-space segments are accepted if the NAV signal is within a prespecified gating window. Otherwise data are discarded and reacquired in the next cardiac cycle. The outer *k*-space data are included only if the data are within the acceptance window, otherwise they will be estimated during the reconstruction.

Utility of compressed sensing (CS) for estimating motion-corrupted data was presented for removing swallowing artifacts in larynx imaging (24). A pseudorandom trajectory was designed to generate a motion-free undersampled *k*-space from the information provided by NAV. The undersampled *k*-space of larynx was then used in the standard CS algorithm (25) to estimate the unfilled *k*-space data. In cardiac MR, the quasiperiodic nature of the respiratory pattern yields a randomly undersampled *k*-space. Therefore, CS reconstruction could potentially be used to estimate the motion-corrupted *k*-space data without reacquiring them. In this study, we have proposed and evaluated a joint retrospective–prospective NAV gating approach, CS motion compensation (CosMo) for coronary MRI. Imaging using a nonrigid motion phantom and in vivo coronary MRI were used to evaluate the efficacy of the proposed respiratory motion technique.

MATERIALS AND METHODS

Figure 1 shows the proposed CosMo data acquisition strategy. The *k*-space segments are divided into inner and outer regions, which are acquired using two different approaches. The inner *k*-space segments are first fully acquired using a diaphragmatic NAV with a predefined gating window, similar to the prospective NAV acquisition. The outer *k*-space segments are accepted for image reconstruction only if the NAV position is within the gating window at the time of their acquisitions; otherwise the *k*-space segments are discarded and not reacquired. On completion of the scan, the inner segments are fully sampled, while the outer *k*-space is undersampled. The pattern of undersampling is enforced by NAV and respiratory motion of a subject. We hypothesize that this undersampling pattern is random, and methods such as CS (25,26) can be used to estimate the motion-corrupted *k*-space segments.

This study is divided into two sections: (1) to investigate the randomness and incoherence of the NAV-generated undersampling pattern and (2) to investigate the efficacy of CosMo for respiratory motion compensation in coronary MRI. Initially, the feasibility of CosMo is studied on a respiratory motion phantom. Then, in a retrospective study, the randomness and incoherence of the generated *k*-space undersampling pattern in 3D coronary MRI with the proposed acquisition strategy is investigated. Finally, the generated undersampling *k*-space data are reconstructed for different gating windows and compared with the images from fully sampled data.

Nonrigid Respiratory Phantom Study

To investigate the feasibility of the proposed method, we first performed a phantom study on our pneumatic MR-compatible respiratory and cardiac motion phantom of a two-chamber deformable human heart. The phantom allows for respiratory motion along superior–inferior and anterior–posterior directions; however, only superior–inferior respiratory motion was used in our experiments. The desired respiratory motion of the phantom, generated from a subject's respiratory motion, was programmed into a microprocessor. The microprocessor controls the motion of the phantom outside the magnet room using a fiber optic cable. The phantom was imaged with an ECG triggered, 3D axial, steady-state free precession sequence with the following parameters: repetition time/echo time = 5.0/2.0 ms; field of view = 300 × 300 × 112 mm^3; spatial resolution 1.3 × 1.3 × 1.5 mm^3; flip angle = 90°. A 2D pencil-beam NAV was placed at the edge of the plate moving the heart, to measure the displacement along superior–inferior direction. The acquisition was obtained using 22 phase-encode lines per segment. At the beginning of the scan, the first 20 cardiac cycles were used as a training phase to define the center of 5 mm gating window. The inner *k*-space lines ($k_y \times k_z$ of 37×26) were fully acquired within this gating window while the outer *k*-space lines were acquired with 100 mm gating window. A centric profile ordering was used for acquiring the inner *k*-space segments. After acquiring the inner *k*-space segments, the profile ordering was changed to the standard radial spokes for acquisition of the rest of *k*-space segments. For outer *k*-space, only data within the acceptance window were used for image reconstruction. A fully sampled reference image with prospective NAV acquisition was also acquired.

Image Reconstruction

After generating the fully sampled and randomly undersampled 3D *k*-space datasets, the undersampled dataset was reconstructed using the modified CS approach (27) called low-dimensional structure self-learning and thresholding (LOST). Minimization of the convex l_1 norm of transform domain coefficients has been the preferred CS sparsity regularization in MRI. This technique assumes that an image has a sufficiently sparse representation in a preselected transform domain. Although sparsity is a necessary condition for l_1 norm reconstruction, it is not possible to know whether a transform can efficiently represent the underlying image characteristics. Furthermore, the relevant anatomical features are not necessarily captured in a sparse manner with a fixed transform. LOST, on the other hand, uses the structure and anatomical features in the image being reconstructed. By using the information from the image itself, it is able to represent various anatomical features of the image sparsely in an adaptive fashion, without the need for training data. This adaptive representation allows for the removal of aliasing artifacts and noise using thresholding approaches, without causing significant reconstruction artifacts and blurring (27). Therefore, in this study, we have used LOST to estimate the motion-corrupted *k*-space segment in CosMo.

The proposed method was implemented in MATLAB (The MathWorks, Natick, MA) and C++ using the FFTW library, for off-line reconstruction. The final estimate is generated by root sum squares of the coil estimates.

Coronary MRI Acquisition

Nine healthy adult subjects (three males, 25 ± 12 years), without any contraindications to MRI, were recruited for this study. All images were acquired using a 1.5 T scanner (Achieva, Philips Healthcare, Best, The Netherlands) and a five-channel phased array coil. Written informed consent was obtained from all the participants, and the imaging protocol was approved by our Institutional Review Board.

In each scan, scout images were acquired to localize the anatomy using a balanced steady-state free precession sequence with 3.1×3.1 mm^2 in-plane resolution and 10 mm slice thickness. On the scout image, a 2D pencil-beam NAV was placed at the dome of the right hemidiaphragm. To measure the coil sensitivity maps, a set of reference images were acquired using both the body and the phased array coils. The coil sensitivity maps were used for subsequent acquisitions but not in LOST reconstruction. The scan was followed by an axial breath-hold cine steady-state free precession sequence with 1.2×1.2 mm^2 in-plane resolution and 48 ms temporal resolution, to visually identify the rest period of the right coronary artery (RCA). A low-resolution 3D coronary survey volume was next acquired to define an oblique imaging slab covering the RCA. The oblique imaging plane was used to acquire a free-breathing 3D ECG-gated steady-state free precession sequence with the following parameters: $270 \times 270 \times 30$ mm^3 field of view; $1.0 \times 1.0 \times 3.0$ mm^3 spatial resolution; echo time/repetition time = 2.6/5.3 ms; flip angle 90°; number of *k*-space segments measured per shot = 17; NAV gating window = 100 mm, i.e., efficiency of 100%; number of averages = 10. Both NAV signal and raw *k*-space data were recorded and transferred to a stand-alone workstation for further retrospective analysis and reconstruction.

NAV-Generated Undersampling

To study the undersampling pattern generated by NAV, we retrospectively analyzed the acquired data. For each subject, we had 10 averages and corresponding NAV positions for each segment. To verify the randomness of the accepted *k*-space segments for each average, a probability map was generated. The probability map shows the acceptance probability of a specific *k*-space segment within a predefined gating window over 10 averages. This probability changes from zero, the case where the *k*-space segment is not acquired over 10 averages, to 1, for the case where the segment is acquired in all the averages. Had the generated undersampling pattern been the same at each average, i.e., a deterministic undersampling pattern, the generated probability map would have only values of either zero or one. Otherwise, if the undersampling pattern was random, the probability map would have values ranging from 0 to 1. In the generated probability map, the *k*-space segments having the probability of 0.5 had the maximum randomness over 10 averages.

We used the sidelobe-to-peak ratio (SPR) (25) to investigate the incoherence of the resulting undersampling pattern. We calculated the point spread functions of the undersampled *k*-spaces generated for 5 mm gating window for each subject. The SPR was then calculated as the ratio of the second highest peak to the maximum peak of the point spread function. A lower SPR suggests an incoherent random sampling pattern. In our analysis, due to the breathing pattern, the gating efficiency for different averages was different. This fact, along with the pattern of the undersampled *k*-spaces, results in different values for SPR (10 per subject for a total of 90 SPR for all subjects).

The probability map and computed SPR, respectively, evaluate the randomness and incoherence of the

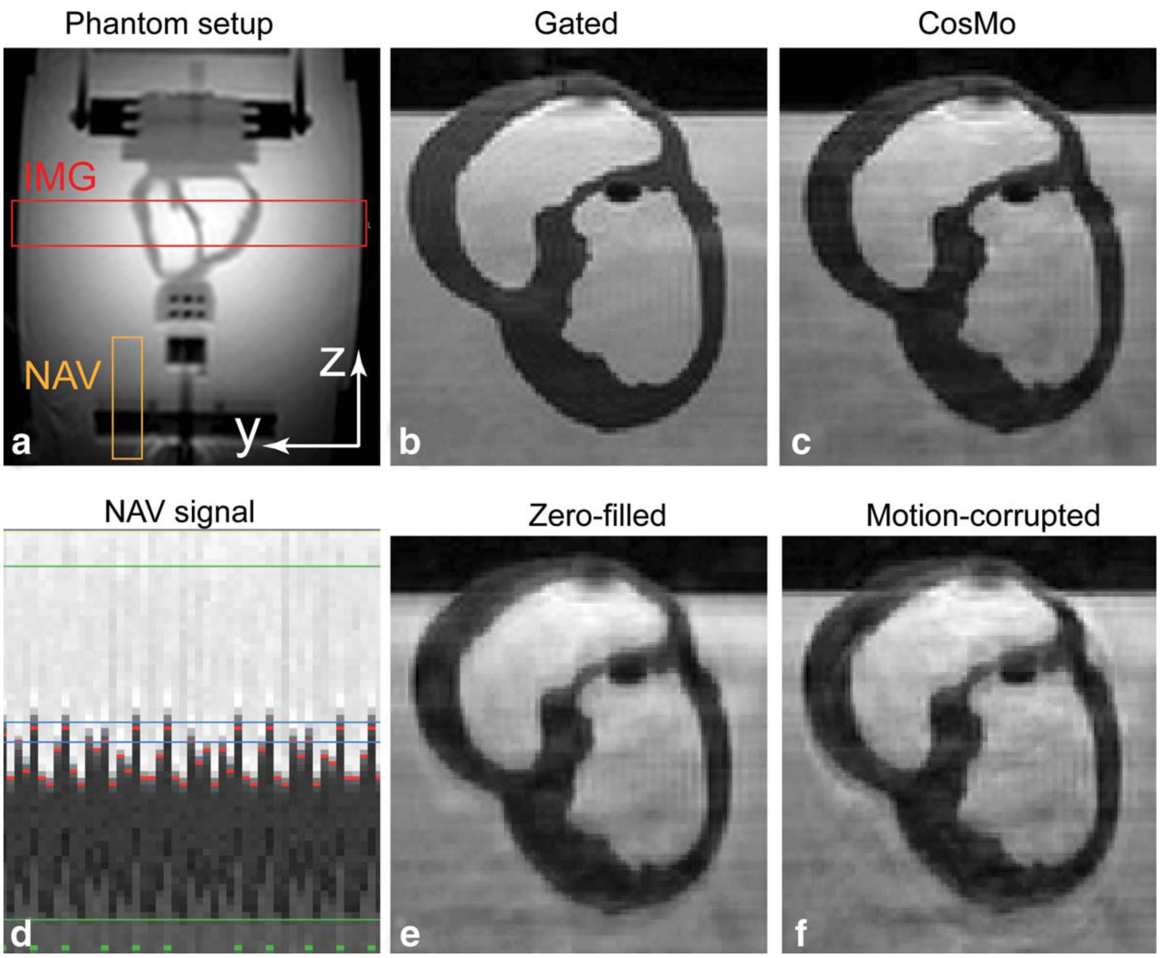

FIG. 2. Nonrigid motion phantom: **a**: 2D image of the phantom setup demonstrating position of the imaging slab and NAV. **b**: NAV signal tracking the heart and acquiring the inner *k*-space lines within 5 mm gating window (after this stage the gating window is increased to acquire the rest of *k*-space lines). Green, red, and blue lines represent the accepted *k*-space segments, measured phantom displacements, and gating window size, respectively. **c**: Prospectively gated NAV with 5 mm gating window. **d**: Zero-filled image, where the outer *k*-space data acquired outside the gating window are replaced with zero. **e**: CosMo reconstructed image using 51% *k*-space data. **f**: Motion-corrupted image, where the outer *k*-space data acquired outside the gating window are used in the image reconstruction. [Color figure can be viewed in the online issue, which is available at wileyonlinelibrary.com.]

undersampling *k*-space patterns that are generated by the respiratory motion measured by NAV.

Retrospective Coronary MRI

A retrospective NAV-gated image dataset was reconstructed as a reference from the acquired datasets. To fill in the *k*-space, *k*-space lines from the first average were included if the associated NAV signal, acquired prior the *k*-space lines, was within the predefined acceptance window determined during a training phase. For the unfilled *k*-space lines in the *k*-space, the data from the subsequent averages were used. The *k*-space contains only one instance of the accepted *k*-space segments from all the nine averages and the remainder of the data was discarded. Four different references were reconstructed for gating windows of 3, 5, 7, and 10 mm. Additionally, another retrospectively gated reference was generated by using a variable gating window of 5 and 10 mm for the inner (the inner 50% of *k*-space) and the outer (the outer 50% of *k*-space) *k*-space segments, respectively.

To create the CosMo *k*-space data, the *k*-space was divided into two regions: inner and outer. For inner region, the *k*-space data were selected similar to the retrospective NAV gated dataset. For outer region, the *k*-space data acquired in the first average was included in the final *k*-space data if it is within the acceptance window, otherwise these segments were unfilled. This procedure results in the *k*-space data, which is fully sampled in the inner region while containing randomly distributed unfilled data in the outer region. Similar to the retrospective data, only one instance of each *k*-space segment was included.

Image Analysis

For each of the nine subjects, we retrospectively reconstructed coronary images by gating the respiratory motion and using CosMo for different gating windows.

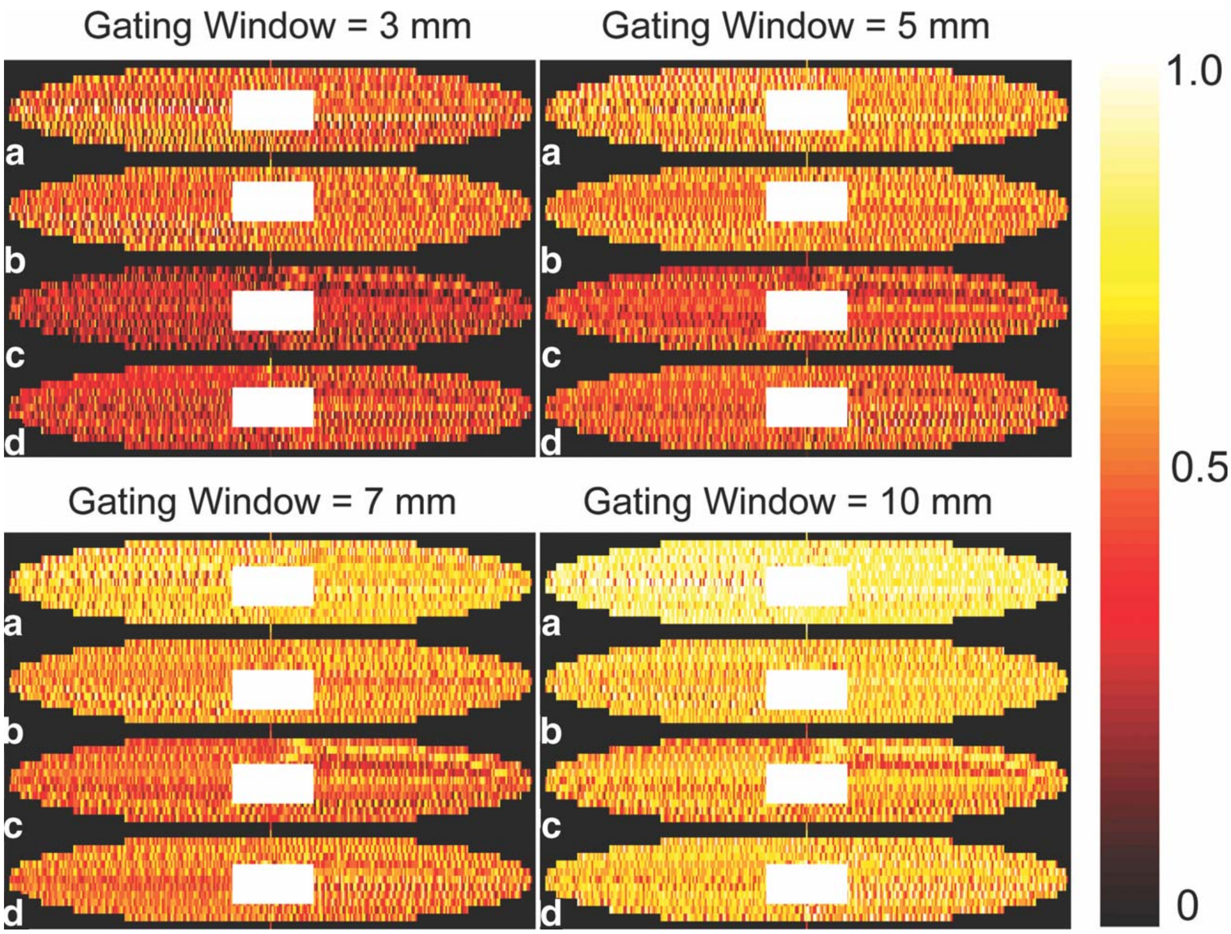

FIG. 3. NAV-generated respiratory undersampling pattern: the color map shows the probability of accepted k_y–k_z segments by NAV of four subjects (A–D) for four gating windows (3, 5, 7, 10 mm). The undersampled lines exhibit randomness between different subjects and for different gating windows.

Qualitative assessment of coronary artery images was performed by an experienced independent blinded reader using a four-point scale system as previously described in Ref. 28: 1, indicating poor or uninterpretable (coronary artery visible, with markedly blurred borders or edges); 2, fair (coronary artery visible, with moderately blurred borders or edges); 3, acceptable (coronary artery visible, with mildly blurred borders or edges); or 4, excellent (coronary artery visible, with sharply defined borders or edges). For each image, separate scores were given for the proximal, mid, and distal segments. The Soap Bubble (29) (Philips Healthcare, Best, The Netherlands) tool was used to quantitatively evaluate the vessel definition. Vessel sharpness scores were calculated for both sides of the vessel, and final sharpness was defined as the average score of the both sides. The final normalized sharpness was defined as the average score of the both sides divided by the lumen signal.

Statistical Analysis

All measurements are presented as mean ± one standard deviation. A two-tailed, paired Student's *t*-test was used for comparing image quality in all the measurements except the visual grading. A paired two-sided Wilcoxon test was performed for the visual grading. A *P* value of <0.05 was considered statistically significant.

RESULTS

Nonrigid Respiratory Phantom Study

Figure 2 depicts the reconstructed images of the respiratory motion phantom using CosMo compared with the prospective NAV gating; zero-filled and motion-corrupted images. CosMo improves visualization of the motion phantom and preserve the sharp edges between the heart and distillated water despite using only 51% of the *k*-space data.

Coronary MRI

Figure 3 shows the NAV-generated probability map of the accepted k_y–k_z lines over 10 averages of four healthy subjects (A–D) for gating windows of 3, 5, 7, and 10 mm, respectively. The undersampled locations exhibit randomness for all subjects at all gating windows. As the size of gating window increases from 3 to 10 mm, the acceptance probability of the outer *k*-space segments also increases.

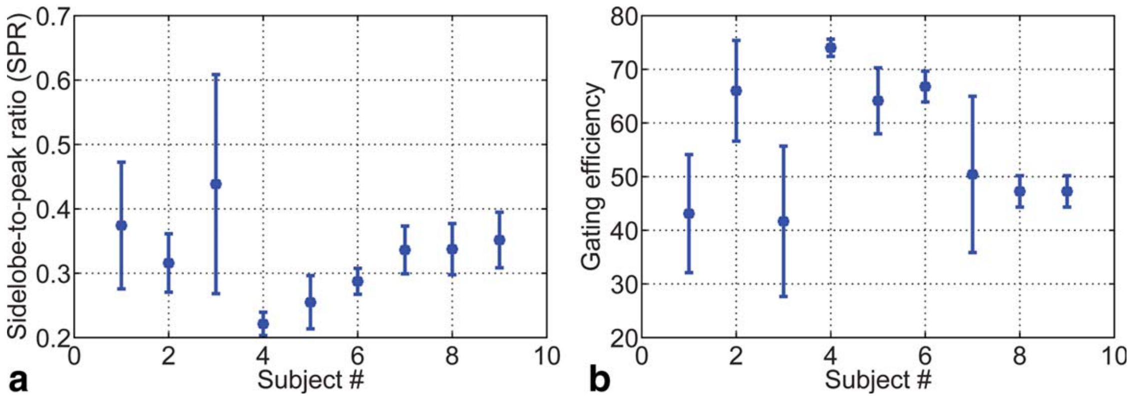

FIG. 4. Mean and standard deviation of the sidelobe-to-peak ratio (SPR) of the undersampled *k*-spaces generated within 5 mm gating window for each subject (**a**), and calculated SPR for calculated gating efficiency (**b**). [Color figure can be viewed in the online issue, which is available at wileyonlinelibrary.com.]

Figure 4a displays the mean and standard deviation of SPR over the 10 undersampled *k*-spaces for each subject. Figure 4b shows the SPR in terms of the gating efficiency of each undersampled *k*-space. Due to the breathing pattern, the gating efficiency differs for different averages and different undersampling pattern is generated. As the gating efficiency reduces, the *k*-space becomes highly undersampled and SPR increases. As a point of comparison, 10 undersampled *k*-space patterns generated by randomly discarding the outer *k*-space region while keeping the central portion of *k*-space (for an acceleration rate of 1.75), has average SPR of 0.27 ± 0.01.

Figure 5 shows the reformatted images using retrospective NAV gating and CosMo for gating windows of 3, 5, 7, 10, and 5/10 mm. In this example, the gating efficiencies for CosMo reconstruction for gating windows of 3, 5, 7, 10, and 5/10 mm were 67%, 73%, 78%, 82%, and 76%, respectively. CosMo images are highly comparable with the fully sampled acquisition. The mean gating efficiencies range from 47% to 76% for different gating window sizes. Despite an improvement in gating efficiency in the images acquired using a larger gating window of 10 mm for outer *k*-space, the subjective score did not deteriorate compared to smaller gating window.

Table 1 summarizes the subjective RCA image scores. There is no significant difference between the scores of the images reconstructed by the retrospective gating of the respiratory motion and CosMo. Table 2 displays the coronary sharpness measure for different gating windows, which demonstrates no significant difference between the retrospective NAV and CosMo.

DISCUSSION

In this study, a joint prospective–retrospective NAV, so called CosMo, is implemented and assessed for coronary MRI. The quasiperiodic nature of subject's breathing is used to generate an undersampled *k*-space. Subsequently, the motion-corrupted *k*-space segments were estimated in the reconstruction step using LOST reconstruction. As CS algorithms require a certain region of inner *k*-space data to be fully acquired, the proposed prospective–retrospective NAV guarantees acquiring those *k*-space lines within the gating window by using a prospective diaphragmatic NAV.

While similar scan time can be achieved with an accelerated acquisition using an acceleration factor of 2–3, CosMo results in a fixed and deterministic scan time.

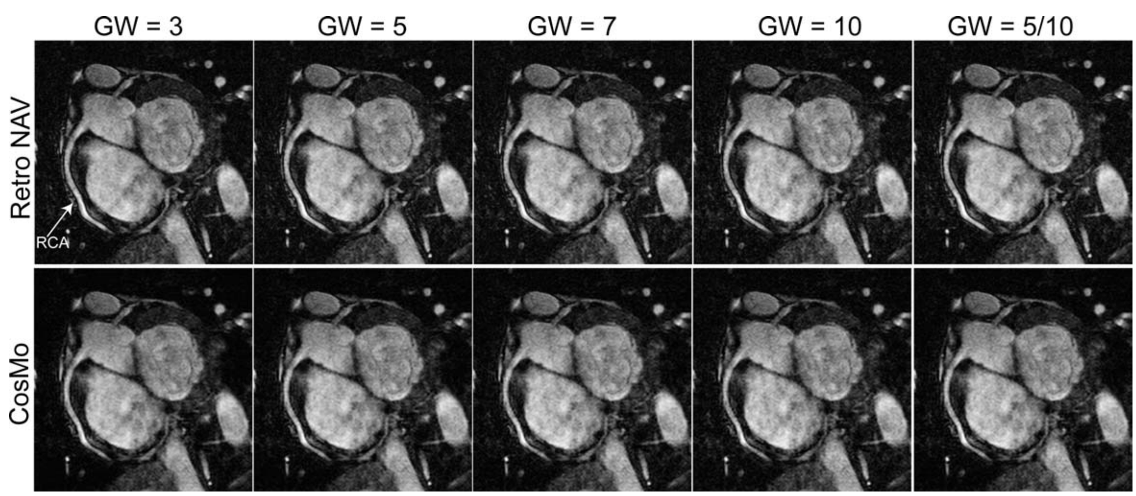

FIG. 5. The reformatted right coronary artery (RCA) images using retrospective NAV and CosMo for different gating windows (GW) of 3, 5, 7, 10 and inner/outer *k*-space of 5/10 mm. Comparable image quality can be seen between CosMo and NAV gated data.

Table 1
Subjective RCA Image Scores for Retrospective NAV and CosMo with Different Gating Windows for Proximal, Mid and Distal Segments

Window size (mm)	NAV technique	Gating efficiency (%)	PROX	MID	DIS
3	Retro NAV	N/A	3.1 ± 0.6	2.9 ± 0.6	2.4 ± 0.8
	CosMo	47	3.1 ± 0.7	2.6 ± 0.9	2.4 ± 0.8
5	Retro NAV	N/A	2.8 ± 0.4	2.9 ± 0.6	2.3 ± 0.4
	CosMo	57	2.8 ± 0.7	2.8 ± 0.8	2.3 ± 0.7
7	Retro NAV	N/A	3.1 ± 0.6	2.9 ± 0.6	2.7 ± 0.7
	CosMo	64	2.6 ± 0.7	2.5 ± 1.0	2.1 ± 0.7
10	Retro NAV	N/A	2.6 ± 0.7	2.6 ± 0.7	2.3 ± 0.7
	CosMo	76	2.5 ± 0.5	2.3 ± 0.8	2.1 ± 0.9
5, 10	Retro NAV	N/A	3.0 ± 0.7	3.0 ± 0.5	2.5 ± 0.5
	CosMo	62	2.8 ± 0.7	2.8 ± 0.8	2.1 ± 0.9

No statistically significant difference was found between the two techniques.

There have been several approaches to combine parallel imaging techniques with CS reconstruction to accelerate acquisition (30). In this study, we did not use any parallel acquisition to allow for evaluation of the proposed method and comprehensive study of the undersampling pattern. However, CosMo can be used with current parallel imaging reconstruction techniques for further reduction in scan time. Further investigation is needed to understand the efficacy of combining CosMo with parallel imaging.

The randomness of the undersampling pattern generated by CosMo was also studied using a probability map and the SPR of the undersampling *k*-space patterns. While the SPR measure provides a rule-of-thumb for the applicability of CS, it is inherently tailored for linear reconstruction methods (31) and is signal independent. Thus, it cannot give a full characterization of the reconstruction process, especially for LOST, which is signal adaptive. Nonetheless, it provides a simple measure for the incoherency of the undersampled *k*-space pattern, and results suggest that the SPR of the pattern generated by CosMo is not very different from that of a randomly generated pattern.

There are significant variations among different patients in terms of breathing pattern and this pattern usually changes during the long scan. In some patients, the undersampling factor enforced by poor respiratory pattern might be too high for reliable image reconstructions. In these cases, alternative approaches should be used to guarantee a minimal amount of outer *k*-space data prior to completion of the scan. While this might increase the scan time, it makes sure that the undersampling will not be too high for image reconstruction. Such approaches need further investigation.

In CosMo, motion-corrupted outer *k*-space data are completely discarded. However, these data may contain useful information that can improve CosMo reconstruction. Respiratory motion contributes to *k*-space errors through a variety of effects, e.g., motion relative to the spatially varying coil sensitivities and nonrigid motion. Nevertheless, the respiratory motion of the heart can be approximated by a time-varying rigid translation. This motion will manifest itself as phase variation in the acquired *k*-space segment. Therefore, *k*-space magnitude still carries some useful information and may be used to improve reconstruction by adding additional constraint on the magnitude of the estimated *k*-space lines. This approach needs to be further studied.

We have used diaphragmatic NAV as a surrogate for respiratory motion. However, other methods such as respiratory bellows or fat NAV may also be used.

Our study has several limitations. We have only compared the CosMo-reconstructed images with a retrospective NAV-gated reconstruction. A prospective NAV gated with tracking is commonly used for coronary MRI. The methodology used in this study to create the reference data closely simulates a prospective acquisition without any correction (tracking) or adaptive gating. However,

Table 2
RCA Sharpness of the Images Reconstructed with Different Gating Windows Using Retrospective NAV and CosMo

Window size (mm)	NAV technique	Gating efficiency (%)	Sharpness	Normalized sharpness
3	Retro NAV	N/A	1865 ± 733	0.54 ± 0.07
	CosMo	47	1537 ± 632	0.5 ± 0.08
5	Retro NAV	N/A	1661 ± 523	0.52 ± 0.08
	CosMo	57	1424 ± 560	0.49 ± 0.09
7	Retro NAV	N/A	1834 ± 695	0.53 ± 0.07
	CosMo	64	1424 ± 560	0.49 ± 0.08
10	Retro NAV	N/A	1778 ± 761	0.51 ± 0.08
	CosMo	76	1512 ± 650	0.48 ± 0.09
5, 10	Retro NAV	N/A	1836 ± 707	0.52 ± 0.08
	CosMo	62	1548 ± 568	0.49 ± 0.08

There was no statistically significant difference between the two techniques with any of gating windows.

gating and tracking will have slightly higher acquisition efficiency compared to gating. Further studies are needed to directly compare the CosMo image acquisition with a prospective NAV gating and tracking. In our current implementation, the size of the fully acquired inner *k*-space segments was empirically determined. Further studies are needed to systematically study the minimum required number of lines. LOST algorithm with its experimentally chosen parameters was used in CosMo to reconstruct the coronary images and we did not systematically investigate how to optimize LOST's individual parameters. We used objective vessel sharpness and subjective image scores as image quality end points. These metrics may not reflect the clinical improvements of atherosclerosis lesion detection.

CONCLUSIONS

CosMo acquisition results in randomly unfilled *k*-space data in coronary MRI that can be estimated in reconstruction step using a CS algorithm, such as LOST, without reacquiring the motion-corrupted data. This approach yields a scan time reduction in coronary MRI.

ACKNOWLEDGMENT

Mehdi H. Moghari acknowledges the fellowship support from NSERC (Natural Sciences and Engineering Research Council of Canada).

REFERENCES

1. Scott AD, Keegan J, Firmin DN. Motion in cardiovascular MR imaging. Radiology 2009;250:331–351.
2. Wang Y, Vidan E, Bergman GW. Cardiac motion of coronary arteries: variability in the rest period and implications for coronary MR angiography. Radiology 1999;213:751–758.
3. Niendorf T, Hardy CJ, Giaquinto RO, Gross P, Cline HE, Zhu Y, Kenwood G, Cohen S, Grant AK, Joshi S, Rofsky NM, Sodickson DK. Toward single breath-hold whole-heart coverage coronary MRA using highly accelerated parallel imaging with a 32-channel MR system. Magn Reson Med 2006;56:167–176.
4. Edelman RR, Manning WJ, Burstein D, Paulin S. Coronary arteries: breath-hold MR angiography. Radiology 1991;181:641–643.
5. Ehman RL, Felmlee JP. Adaptive technique for high-definition MR imaging of moving structures. Radiology 1989;173:255–263.
6. Taylor AM, Jhooti P, Wiesmann F, Keegan J, Firmin DN, Pennell DJ. MR navigator-echo monitoring of temporal changes in diaphragm position: implications for MR coronary angiography. J Magn Reson Imaging 1997;7:629–636.
7. Wang Y, Rossman PJ, Grimm RC, Riederer SJ, Ehman RL. Navigator-echo-based real-time respiratory gating and triggering for reduction of respiration effects in three-dimensional coronary MR angiography. Radiology 1996;198:55–60.
8. Sachs TS, Meyer CH, Hu BS, Kohli J, Nishimura DG, Macovski A. Real-time motion detection in spiral MRI using navigators. Magn Reson Med 1994;32:639–645.
9. Oshinski JN, Hofland L, Mukundan S Jr, Dixon WT, Parks WJ, Pettigrew RI. Two-dimensional coronary MR angiography without breath holding. Radiology 1996;201:737–743.
10. Nguyen TD, Spincemaille P, Prince MR, Wang Y. Cardiac fat navigator-gated steady-state free precession 3D magnetic resonance angiography of coronary arteries. Magn Reson Med 2006;56:210–215.
11. Keegan J, Gatehouse PD, Yang GZ, Firmin DN. Non-model-based correction of respiratory motion using beat-to-beat 3D spiral fat-selective imaging. J Magn Reson Imaging 2007;26:624–629.
12. Jhooti P, Keegan J, Firmin DN. A fully automatic and highly efficient navigator gating technique for high-resolution free-breathing acquisitions: continuously adaptive windowing strategy. Magn Reson Med 2010;64:1015–1026.
13. Lai P, Bi X, Jerecic R, Li D. A respiratory self-gating technique with 3D-translation compensation for free-breathing whole-heart coronary MRA. Magn Reson Med 2009;62:731–738.
14. Pipe JG. Motion correction with propeller MRI: application to head motion and free-breathing cardiac imaging. Magn Reson Med 1999; 42:963–969.
15. Stehning C, Bornert P, Nehrke K, Eggers H, Stuber M. Free-breathing whole-heart coronary MRA with 3D radial SSFP and self-navigated image reconstruction. Magn Reson Med 2005;54:476–480.
16. Schmidt JF, Buehrer M, Boesiger P, Kozerke S. Highly efficient respiratory gating in whole heart MR employing non-rigid retrospective motion correction. In: Proceedings of the 18th Annual Meeting of ISMRM, Stockholm, Sweden; 2010.
17. Hardy CJ, Zhao L, Zong X, Saranathan M, Yucel EK. Coronary MR angiography: respiratory motion correction with BACSPIN. J Magn Reson Imaging 2003;17:170–176.
18. Bhat H, Ge L, Nielles-Vallespin S, Zuehlsdorff S, Li D. 3D projection reconstruction based respiratory motion correction technique for free-breathing coronary MRA. In: Proceedings of the 18th Annual Meeting of ISMRM, Stockholm, Sweden; 2010.
19. Sachs TS, Meyer CH, Pauly JM, Hu BS, Nishimura DG, Macovski A. The real-time interactive 3-D-DVA for robust coronary MRA. IEEE Trans Med Imaging 2000;19:73–79.
20. Manke D, Nehrke K, Bornert P. Novel prospective respiratory motion correction approach for free-breathing coronary MR angiography using a patient-adapted affine motion model. Magn Reson Med 2003;50:122–131.
21. Nehrke K, Bornert P. Prospective correction of affine motion for arbitrary MR sequences on a clinical scanner. Magn Reson Med 2005;54: 1130–1138.
22. O'Connor AC, Moghari MH, Hu P, Peters DC, Manning WJ, Nezafat R, Brockett RW. Retrospective motion-adapted smart averaging for free-breathing cardiac MRI. In: Proceedings of the 18th Annual Meeting of ISMRM, Stockholm, Sweden; 2010.
23. Weiger M, Bornert P, Proksa R, Schaffter T, Haase A. Motion-adapted gating based on k-space weighting for reduction of respiratory motion artifacts. Magn Reson Med 1997;38:322–333.
24. Barral JK, Nishimura DG. Compressed sensing for motion artifact reduction. In: Proceedings of the 17th Annual Meeting of ISMRM, Honolulu, Hawaii; 2009. p 4593.
25. Lustig M, Donoho DL, Pauly JM. Sparse MRI: the application of compressed sensing for rapid MR imaging. Magn Reson Med 2007;58: 1182–1195.
26. Block KT, Uecker M, Frahm J. Undersampled radial MRI with multiple coils. Iterative image reconstruction using a total variation constraint. Magn Reson Med 2007;57:1086–1098.
27. Akcakaya M, Basha T, Goddu B, Goepfert L, Kissinger KV, Tarokh V, Manning WJ, Nezafat R. Low-dimensional-structure self-learning and thresholding (LOST): regularization beyond compressed sensing for MRI reconstruction. Magn Reson Med 2011 [Epub ahead of print.].
28. Kim WY, Danias PG, Stuber M, Flamm SD, Plein S, Nagel E, Langerak SE, Weber OM, Pedersen EM, Schmidt M, Botnar RM, Manning WJ. Coronary magnetic resonance angiography for the detection of coronary stenoses. N Engl J Med 2001;345:1863–1869.
29. Etienne A, Botnar RM, Van Muiswinkel AM, Boesiger P, Manning WJ, Stuber M. "Soap-Bubble" visualization and quantitative analysis of 3D coronary magnetic resonance angiograms. Magn Reson Med 2002;48:658–666.
30. Lustig M, Pauly JM. SPIRiT: iterative self-consistent parallel imaging reconstruction from arbitrary k-space. Magn Reson Med 2010;64:457–471.
31. Seeger M, Nickisch H, Pohmann R, Scholkopf B. Optimization of k-space trajectories for compressed sensing by Bayesian experimental design. Magn Reson Med 2010;63:116–126.